Unerosion: Simulating Terrain Evolution Back in Time
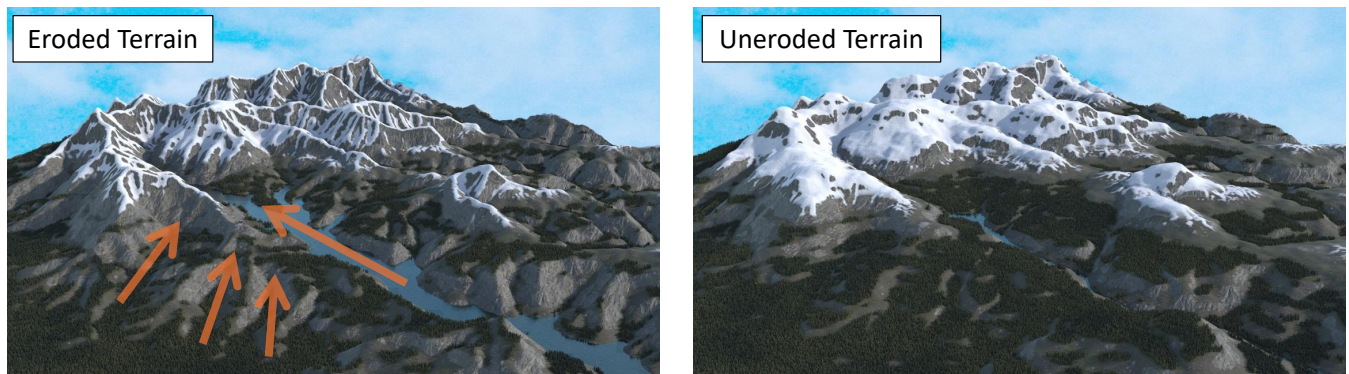
Zhanyu Yang[1] , Guillaume Cordonnier[2] , Marie-Paule Cani[3] , Christian Perrenoud[4] and Bedrich Benes[1]

[1]Purdue University, USA
[2]Inria, Université Côte d'Azur, France
[3]LIX, École Polytechnique and CNRS, IP Paris, France
[4]Histoire Naturelle de l'Homme Préhistorique, France

Figure 1: *A terrain that has been eroded (left) by fluvial and thermal erosion is uneroded by automatically tracing the direction of the main flow (indicated by the arrows) to its previous state.*

Abstract
While the past of terrain cannot be known precisely because an effect can result from many different causes, exploring these possible pasts opens the way to numerous applications ranging from movies and games to paleogeography. We introduce unerosion, an attempt to recover plausible past topographies from an input terrain represented as a height field. Our solution relies on novel algorithms for the backward simulation of different processes: fluvial erosion, sedimentation, and thermal erosion. This is achieved by re-formulating the equations of erosion and sedimentation so that they can be simulated back in time. These algorithms can be combined to account for a succession of climate changes backward in time, while the possible ambiguities provide editing options to the user. Results show that our solution can approximately reverse different types of erosion while enabling users to explore a variety of alternative pasts. Using a chronology of climatic periods to inform us about the main erosion phenomena, we also went back in time using real measured terrain data. We checked the consistency with geological findings, namely the height of river beds hundreds of thousands of years ago.

CCS Concepts
• *Computing methodologies* → *Shape modeling;*

Keywords: Terrain, Erosion, Simulation of Natural Phenomena

1. Introduction

Traveling back in time has always been a dream of humankind. Many books and films feature time travelers who materialize at different points in time while remaining in the same place. Others span extensive periods of time with the history or depict a certain location centuries or even thousands of years ago. Concurrently, historians, archaeologists, and paleontologists study past civilizations or ancient species, and they try to retrieve the environment where they developed, particularly the former locations of coastlines and rivers. Geologists typically explore former states of terrains over larger time periods, spanning up to tectonic plate motion and the formation of continents. We contribute to this effort by enabling the

exploration of plausible past states of terrain, up to medium-scale periods of several millions of years.

Computing the past of terrain is a challenging and ill-posed problem depending on many more or less known factors. The first one is the environmental conditions to which the explored terrain was subjected. In particular, climatic changes induced different natures and strengths of the main erosion phenomena, and the erosion was also heavily affected by vegetation cover under these different climates, which is vastly unknown. The second factor is the local effect of larger-scale geological phenomena, such as continental plate movements, terrain folding, and volcanology, which may have induced specific variations in the terrain uplift rates throughout the study. Another factor is the input terrain's present and past geological constituents. The volumetric nature of Earth's crust changes the top layer over time as it undergoes erosion and deposition. This change of ground material induces changes in erosion rates. The terrain erosion processes also have varying speeds. Floods and downpours affect terrain quickly, while thermal erosion is significantly slower. Lastly, backward erosion is an ill-posed problem because even if all these factors were known precisely, simulating the terrain evolution back in time would not give a single solution. Indeed, a rock encountered in the middle of a valley could have fallen from many possible locations. In general, there is an infinite number of possible past terrains that could have eroded into the one we observe nowadays. We aim to offer a tool that allows exploring a variety of possible pasts rather than focusing on just one of them.

We introduce a simulation method enabling users to easily explore some of the possible pasts of a terrain defined as a height map from only a few hypotheses about the main climatic changes and the amount of local uplift it underwent over time. This is achieved by re-formulating the equations of erosion and sedimentation so that they can be simulated back in time, a process that we call "unerosion", and by proposing a way to combine them over a timeline of former climatic periods. Meanwhile, the nature of the ground and its change over time can be tuned by the user to explore a variety of results.

Our main contributions are (1) A solution for fluvial unerosion, which we apply to a new model augmented with sedimentation, inspired by recent work in geology; (2) A new formulation of thermal erosion enabling solving for thermal unerosion thanks to a stable numerical scheme; (3) A conversion between a chronology of past climatic periods and the main erosion phenomena, enabling us to start from a terrain captured today and go back up to several millions of years.

We present several validation experiments. First, we validate each unerosion model independently by showing that starting from a terrain and uneroding it, our method enables us to return to the same terrain through erosion with negligible error. Second, we illustrate user control by showing how users can explore different plausible pasts of terrain at short to larger time scales (see Fig. 1). Finally, we provide two case studies conducted with a geologist showing that by applying our model at a larger time scale on modern terrains and simulating climatic changes back in time, our method can explain the field findings about the height of river banks at prehistoric times, while enabling to explore possible to-

pographies for the surrounding terrain, a critical benefit for archeologists.

2. Related Work

Terrain modeling attracted a lot of interest from the Computer Graphics community for a very long time (see [GGP*19] for a survey). Most recent methods either focused on deep neural models for terrains or interactive user control [PPB*23; GDG*17; ZLB*19; RKČ*22; SPF*23]. In contrast, our goal is to retrieve the past states of terrain from its current form, a problem that has never been tackled and for which data is lacking. Therefore, we focus below on physically-based methods for simulating terrain formation, i.e., the algorithms we wish to invert.

The main terrain framing processes are related to material transportation, and they can be roughly divided into two main categories: erosion caused by thermal shocks (thermal erosion) and flow of water (fluvial or hydraulic erosion). Several authors addressed the computational requirements by implementing some of the following physics-based algorithms on the GPU [ASA07; MDH07; VBHS11; NWD05; SBK09].

Thermal Erosion: Musgrave et al. [MKM89] made an important observation that fractal terrains lack realism because they do not capture land-forming processes, and they introduced simple cellular-automaton-based thermal erosion. This model was later extended to work on layered data structures [BF01], which was recently extended to quadtrees [GRP*21].

Hydraulic and Fluvial Erosion: The same work that introduced the first thermal erosion [MKM89] also introduced hydraulic erosion that abrades and deposits material. This work was extended into different domains, including approximate fluid dynamics with shallow water [Ben07], smoothed particle hydrodynamics [KBKŠ09], voxels [BTHB06], interaction with layers [ŠBBK08], and even to simulate corrosion [WCMT07]. Hydraulic erosion was also used to simulate rivers that formed terrain in [GGG*13].

Fluvial erosion is a concept coined in geomorphology [WT99; BW13], which is more physically accurate than hydraulic erosion at the scale of mountains and is also the topic of this work. The key concept of fluvial erosion is the water flow and discharge conceptualized into drainage areas. However, the drainage areas do not accurately capture variations in precipitation. Therefore, we replace it with a more accurate computation of the discharge. Fluvial erosion was successfully combined with mountain ranges uplifting at much larger time scales [CBC*16; SPF*23].

Other Factors: The above-described erosion models often act on homogenous terrains, regardless of climate. Several methods considered other factors such as vegetation coverage [CGG*17], glacial erosion [CJP*23], and wind erosion [KHM*20].

Geology: In this paper, given the time scale we are interested in, we focus on thermal and fluvial erosion phenomena while enhancing the former with sedimentation, using a model from geology [YBG*19]. Studying the past states of the earth's crust is a long-lasting problem in geology [Gro99]. Reconstructing volumetric earth-crust and simulating it backward in time through

successive un-sedimentation, un-faltering, and unfolding operations [EHS00; YM03] is, for instance, a key issue for finding underground hydrocarbon reservoirs. While they involve high computational resources, the number of unknowns and the ill-posed nature of the problem make the results highly approximate, as shown by the number of unsuccessful diggings in the hydrocarbons industry. Computer Graphics research helped by enabling expert users to stay in the loop thanks to interactive tools either focused on the sketch-based reconstruction of subsurface geology or the exploration of possible backward simulation scenarios [ABSC14; LNP*12; GCR*18]. Several of these algorithms and tools only considered 2D, vertical cross-sections of a volumetric terrain model.

In contrast, we do not tackle volumetric earth crust simulation, which would be mandatory to achieve backward simulation over longer time scales. Instead, we focus on enabling users to explore a variety of possible pasts for a current 3D terrain, defined as a height field and supposed to have been formed by the combined action of uplift, erosion, and sedimentation.

3. Fluvial Phenomena

The erosion by water, or *fluvial erosion*, is one of the leading causes of landscape formation. It orchestrates the distribution of mountain peaks and the profile of valleys [BFH92] by draining material that may later sediment down-slope.

While fluvial erosion was already simulated in Computer Graphics (Sect. 2), previous models only captured the abrasive effect of flowing water. Sedimentation phenomena cannot be neglected to simulate real terrains backward in time. Therefore, our first contribution is to augment fluvial erosion with sedimentation. Second, using the same differential equation with a negative time step is insufficient for a stable, backward simulation. In graphics and geology, the numerical scheme for fluvial erosion only ensures stability for positive time steps. Moreover, this scheme is dispersive, meaning that even with stable integration, the unerosion would not just undo erosion, preventing users from going back and forth in time and thus making control difficult.

3.1. Complementing Fluvial Erosion with Sedimentation

3.1.1. Fluvial erosion

Previous work [CBC*16; SPF*23] simulated fluvial erosion using a *detachment-limited* erosion model, the Stream Power Law [WT99], which only models the abrasive power of the shear stress of rivers

$$\frac{\partial h}{\partial t} = U - KQ^m \|\nabla h\|^n, \tag{1}$$

where U is a space-time varying uplift function, K is an empirical fluvial erosion coefficient, Q is the water discharge, $\|\nabla h\|$ is the local topographic slope of the heightfield h, t is the time, and m and n are power-law exponents, which depend on the type of terrain. Geomorphology studies agree that only the ratio m/n is relevant and usually set to $m = 0.4$ and $n = 1$ (see Tab. 2 for the notations and parameter values).

Assuming an infinitely thin river, water discharge at a point **p** is:

$$Q(\mathbf{p}) = \iint_{\Omega(\mathbf{p})} p \, dS, \tag{2}$$

with p the local precipitation rate and $\Omega(\mathbf{p})$ is the area spanning all points **q** upstream of **p**, i.e., such that there exists a path of strictly decreasing elevations between **q** and **p**. We deviate here from the approximation from [CBC*16], where discharge was replaced by the drainage area A. Indeed, this is only equivalent when the precipitation rate p is uniformly set to 1m/year.

3.1.2. Adding sediment deposition

The above-mentioned *detachment-limited* assumption is only valid for tectonically active regions without sudden changes in tectonics, climate, or topography (e.g., excluding landslides) [Whi04]. This restrictive condition is rarely encountered in present-day mountains in which many slopes are affected by *transport-limited* erosion, where sediments are deposited when their fluxes exceed the transport capacity of a river.

Departing from previous models, we borrow an extension from geomorphology [YBG*19] that encompasses the *detachment-limited* and the *transport-limited* erosion and deposition

$$\frac{\partial h}{\partial t} = U - KQ^m \|\nabla h\|^n + \frac{K_d}{Q} Q_s, \tag{3}$$

where the sediment discharge Q_s is obtained by integrating the upstream net erosion and using a deposition coefficient K_d, which is a function of the size of the transported sediment grains and the sediment settling velocity. It is often treated as a constant in geomorphology.

$$Q_s(\mathbf{p}) = \iint_{\Omega(\mathbf{p})} U - \frac{\partial h}{\partial t} \, dS. \tag{4}$$

Note that we deviate here from the notations used in [YBG*19], which includes the mean precipitation in their deposition coefficient G since they consider the drainage area (common in geology). Drainage area refers to the geographic zone from which all the precipitation and runoff water flows into a single common outlet. We prefer a formulation that more accurately accounts for local precipitation variations and, therefore, set up our model using discharge, which is the volumetric flow rate of rivers or, equivalently, the upstream integral of the precipitation rate. However, we can still parameterize it from geological measurements by replacing the original deposition coefficients in [YBG*19] with $K_d = G/\bar{p}$ where $\bar{p}$ is the mean precipitation.

3.2. Unified Algorithm for Erosion and Unerosion

With our new reversible algorithm, the only difference between erosion and unerosion is how we discretize the slope.

3.2.1. Computing water and sediment discharge

Our inspiration for the efficient computation of the drainage area comes from the previous work [CBC*16; SPF*23; BW13], which computes the discharge Q from Eqn. (2) recursively as

$$Q(\mathbf{p}) = p(\mathbf{p}) \Delta x^2 + \sum_{\mathbf{q} \in \mathcal{D}(\mathbf{p})} \alpha(\mathbf{q}, \mathbf{p}) Q(\mathbf{p}), \tag{5}$$

where Δx is the cell size of the terrain represented as a regular height field, $\mathcal{D}(\mathbf{p})$ is the set of *donors* of **p** which are among the eight direct Moore's neighbors of **p** and strictly above **p**,

and $\alpha(\mathbf{q}, \mathbf{p})$ is the proportion of the discharge at cell $\mathbf{q}$ that flows toward cell $\mathbf{p}$. We follow [SPF*23] and use a multi-receiver setup

$$\alpha(\mathbf{q}, \mathbf{p}) = \frac{sl(\mathbf{q}, \mathbf{p})}{\sum_{\mathbf{r} \in \mathcal{R}(\mathbf{q})} sl(\mathbf{r}, \mathbf{q})}, \qquad (6)$$

where $sl(\mathbf{q}, \mathbf{p}) = (h(\mathbf{q}) - h(\mathbf{p}))/\|\mathbf{q} - \mathbf{p}\|$ is the slope between $\mathbf{q}$ and $\mathbf{p}$ and $\mathcal{R}(\mathbf{q})$ the set of *receivers* of $\mathbf{q}$, i.e. the set of direct neighbours of $\mathbf{q}$ strictly below $\mathbf{q}$.

We use a similar recursive formulation to compute the sediment discharge Q_s from Eq. (4), replacing $p(\mathbf{p})$ in Eq. (5) by the local net erosion, discretized in time

$$Q_s(\mathbf{p}, t + \Delta t) = \left(U(\mathbf{p}) - \frac{h(\mathbf{p}, t + \Delta t) - h(\mathbf{p}, t)}{\Delta t} \right) \Delta x^2 + \tilde{Q}_s(\mathbf{p}, t + \Delta t), \quad (7)$$

where $\tilde{Q}_s(\mathbf{p}) = \sum_{\mathbf{q} \in \mathcal{D}(\mathbf{p})} \alpha(\mathbf{q}, \mathbf{p}) Q_s(\mathbf{p})$ is the upstream sediment discharge.

3.2.2. Time-discretization for erosion plus deposition

We discretize in time the erosive part of Eq. (3) using a forward Euler explicit scheme, while we treat the deposition term implicitly to improve stability:

$$\frac{h(\mathbf{p}, t + \Delta t) - h(\mathbf{p}, t)}{\Delta t} = U(\mathbf{p}) - K Q(\mathbf{p}, t)^m \|\nabla h(\mathbf{p}, t)\|^n + \\ + \frac{K_d}{Q(\mathbf{p}, t)} \tilde{Q}_s(\mathbf{p}, t + \Delta t). \qquad (8)$$

Note that $\tilde{Q}_s(\mathbf{p}, t + \Delta t)$ only depends on $h(\mathbf{q}, t + \Delta t)$ at positions $\mathbf{q}$ strictly above $\mathbf{p}$. Therefore, with a topological sort of elevations, we can order the computation from top to bottom and interleave Eqs. (7, 8) in a single pass. We start with $\tilde{Q}_s = 0$ for the local maxima of the topography, then iterate over the nodes at position $\mathbf{p}$ in descending order.

Algorithm 1 Algorithm of Fluvial (Un)erosion

Input: $h(t)$
Output: $h(t + \Delta t)$
1: Initialize $\tilde{Q}_s(t)$ as 0;
2: Sort $h(t)$ by height value;
3: **for p** in the descending order of $h(\mathbf{p}, t)$ **do**
4:     Compute $Q(\mathbf{p}, t)$ from Eq. (5);
5:     **if p** not the local maxima of the topology **then**
6:         Compute $\tilde{Q}_s(\mathbf{p}, t + \Delta t)$ from Q_s upstream;
7:     **end if**
8:     Compute $h(\mathbf{p}, t + \Delta t)$ from Eq. (8);
9:     Update $Q_s(\mathbf{p}, t + \Delta t)$ from Eq. (7);
10: **end for**
11: **return** Outputs

3.2.3. Spatial discretization

Eq. 3 is a non-linear Hyperbolic Partial Differential Equation requiring an upwind stability scheme. In other words, we need to offset the computation of gradients in the direction from which the information comes. In erosion processes, the information comes from downstream (for instance, lowering a node on the terrain will

not impact the nodes below but only the nodes above). Therefore, we compute the slopes downstream for erosion

$$\frac{\partial h}{\partial x}^{down}(x, y) = \frac{\max(0, h(x) - h(x + dx), h(x) - h(x - dx))}{dx}, \quad (9)$$

and proceed the same way for $\partial h / \partial y$. This give us the $\|\nabla h(\mathbf{p}, t)\|$ term in Eq. 8).

For un-erosion and the reverse of sedimentation, a process we call *un-deposition*, we use the negative time step to compute height h. The negative Δt is equivalent to using a positive Δt and negatives uplift term U, erosion coefficient K, and deposition coefficient K_d. This inverses the order from which the information comes, and therefore, we need to compute the gradient upstream

$$\frac{\partial h}{\partial x}^{up}(x, y) = \frac{\max(0, h(x + dx) - h(x), h(x - dx) - h(x))}{dx} \quad (10)$$

and similarly for $\partial h / \partial y$. Unfortunately, this scheme is known to be very diffusive, i.e., if we erode a terrain and unerode it back, unerosion results would quickly diverge from the expected non-eroded terrain. While unstable, the alternative-centered scheme is more accurate

$$\frac{\partial h}{\partial x}^c(x, y) = \frac{h(x + dx) - h(x - dx)}{2dx}. \qquad (11)$$

Therefore, we use a slope limiter to interpolate between the stable upwind gradients and the accurately centered ones:

$$\frac{\partial h}{\partial x} = \frac{\partial h}{\partial x}^{up} - \phi\left(\frac{\frac{\partial h}{\partial x}^{down}}{\frac{\partial h}{\partial x}^{up}} \right) \left(\frac{\partial h}{\partial x}^{up} - \frac{\partial h}{\partial x}^c \right), \qquad (12)$$

where the slope limiter function ϕ is set, in our implementation, to the minmod limiter function $\phi(r) = \mathrm{clamp}(r, 0, 1)$. We use the ratio of successive gradients as the parameter of the slope limiter, as this ratio indicates the local stability of the scheme.

4. Thermal Phenomena

Fluvial erosion fails to explain the formation of low drainage regions in the vicinity of peaks and ridges, where other processes dominate [LD03]. For these regions associated with steep slopes, we use *thermal erosion*, a term coined in Computer Graphics (Sect. 2), to model the granular behavior of the mountains at geological scales. It describes a phenomenon where rocks detach above a critical slope, fall, and stabilize in lower areas. However, since this type of erosion is usually not implemented using a differential equation, reverting it in time is even more intricate than fluvial erosion. Therefore, we reformulate the thermal erosion below before discussing unerosion.

4.1. Thermal Erosion

Thermal erosion is a term coined by MUSGRAVE, KOLB, and MACE [1989] as a general term for any gravity-related geomorphological phenomena. While this is not backed by geological evidence, we will use this term as initially proposed. Thermal erosion is usually modeled as a cellular automaton with two layers: the terrain height and the "falling rock" layer. The content in the falling rock layers is transported down if the slope is above the talus angle and is deposited. In particular, if the slope between two cells s

exceeds a talus angle θ, the thermal erosion moves a proportion of $s - \tan\theta$ from the upstream cell in the heightmap layer to the downstream cell in the falling rock layer.

We observe that in the absence of uplift, computing the downstream transport of falling rock is quite similar to the computation of the water or sediment discharges (Eqs. 5 and 7). Therefore, the intermediate rock layer holds a rock discharge Q_r defined as:

$$Q_r(\mathbf{p}) = \iint_{\Omega(\mathbf{p})} -\frac{\partial h}{\partial t}\, dS, \qquad (13)$$

where here $\partial h/\partial t$ is only the elevation change due to thermal erosion. Based on this observation, we can describe a thermal erosion/deposition equation in a form similar to Eq. 3:

$$\frac{\partial h}{\partial t} = -K_{th}\max(0, \|\nabla h\| - \tan\theta) + K_{thd}\,Q_r, \qquad (14)$$

where K_{th} depends on the temperature variations. We increase it in glacial periods, where the temperature often oscillates around 0°C.

However, contrary to fluvial erosion, deposition happens if and only if the slope is below the talus angle. Therefore, we set

$$K_{thd} = 0 \quad \text{if} \quad \|\nabla h\| - \tan\theta > 0.$$

Otherwise, we choose a value such that the maximum amount of sediments are deposited while staying below the critical slope.

After discretizing in time, this yields

$$h(t+\Delta t) = h(t) + \begin{cases} -\Delta t\, K_{th}(\|\nabla h\| - \tan\theta) & \text{if } \|\nabla h\| > \tan\theta, \\ \min(\Delta t \tilde{Q}_r/\Delta x^2, \Delta x(\tan\theta - \|\nabla h\|)) & \text{otherwise,} \end{cases}$$
$$(15)$$

where $\tilde{Q}_r(\mathbf{p}) = \sum_{\mathbf{q}\in\mathcal{D}(\mathbf{p})}\alpha(\mathbf{q},\mathbf{p})Q_r(\mathbf{p})$ is the upstream rock discharge, similarly to the sediment discharge Q_s.

4.2. Constraining Un-Deposition

Thanks to our new formulation for thermal erosion (Eq. 14), we can implement thermal unerosion similarly to fluvial unerosion. However, an issue arises for un-deposition, i.e., when the erosion algorithm would predict an increase in elevation, and therefore, we are computing a decrease of elevation back in time.

The main difference between fluvial and thermal deposition is that thermal deposition is only bounded by the available amount of broken rocks. This means that un-deposition could theoretically assume that all deposition occurred in a single cell, resulting in a deep, single-cell pit.

To prevent this, we observe the behavior of thermal deposition and deduce constraints for un-deposition. During un-erosion, at a time t, we go backward in time with a timestep $-\Delta t$ to compute the terrain at time $t - \Delta t$. Let us assume we are un-depositing on a cell with a downstream slope S_d at time t (computed with Eq. 9). We construct the first constraint from the observation that un-deposition should not carve holes in the ground

$$h(t-\Delta t) - h(t) > -\Delta x\, S_d.$$

However, we observed that when used alone, this constraint creates flat un-deposition terraces, while thermal erosion tends to deposit with a gentle slope. Therefore, we also control a progressive

change of slope in the un-deposition region with a parameter α, which gives the constraint:

$$h(t-\Delta t) > h(t) - \alpha\,\Delta x\, S_d, \qquad (16)$$

where S_d is the norm of the topological gradient.

Another unknown from our data is the geometry of the cliff below the deposited rocks. Therefore, nothing prevents un-deposition from leaving a perfectly vertical wall at the interface between un-erosion and un-deposition. We observe that the bottom of most mountains is convex; therefore, we add a second convexity criterion *upstream* of the eroded location. We set

$$\mathbf{m} = \frac{\left(\frac{\partial h_{ij}}{\partial x}{}^{up}, \frac{\partial h_{ij}}{\partial y}{}^{up}\right)}{\left\|\frac{\partial h_{ij}}{\partial x}{}^{up}, \frac{\partial h_{ij}}{\partial y}{}^{up}\right\|^1},$$

And define

$$f(h_{ij}) = |\mathbf{m}_x|h_{i-sgn(\mathbf{m}_x),j} + |\mathbf{m}_y|h_{i,j-sgn(\mathbf{m}_y)},$$
$$f^2(h_{ij}) = |\mathbf{m}_x|f(h_{i-sgn(\mathbf{m}_x),j}) + |\mathbf{m}_y|f(h_{i,j-sgn(\mathbf{m}_y)}),$$

where *sgn* is the sign function. Then, the slope constraint is:

$$h(t-\Delta t) > 2f(h_{ij})(t-\Delta t) - f^2(h_{ij})(t-\Delta t). \qquad (17)$$

5. Full Backward Simulation from Climate

In general, independently simulating fluvial and thermal erosion back in time is insufficient to explore the past of terrain because the two phenomena should be interleaved. However, it is challenging since the amount of each at a given time highly depends on the climate and is widely unknown. We consider how a plausible simulation can be performed over time periods of several hundreds of thousands of years, given a hypothesis on the local succession of climatic periods during this time range.

5.1. Main Erosion Phenomena from Climate

Earth has experienced cycles of glacial and interglacial periods about every 100 kyr in the last 800 kyr, with the glacial period typically lasting around 80 kyr and the following interglacial period lasting about 20 kyr. While the beginning of the glacial periods shows a progressive cooling of the Earth, during which—in short—some ocean water freezes and the sea level decreases, its end consists of a much faster warming phase. In the study below, inspired from [BE14], we discuss temperate regions on Earth that were not under glaciers during glacial periods (the latter are out of the scope of this paper). The reconstruction of their past average yearly mean temperature typically fluctuates between 2.5°-18.5°C (15.6°C nowadays).

5.1.1. Glacial periods

The cold and dry climate typically results in scarce, prairie-like vegetation coverage. Harsh climatic conditions with frequent freeze and thaw, wind, or snow erode the exposed cliffs, which leads to the deposition of blocks and broken rocks in the mountainous regions upstream of rivers. We model this effect by increasing thermal erosion. The sea level decreases by about 150 meters (at its maximum),

which strongly increases the river slopes and their incision by fluvial erosion: streams carve their bed into the rock layer and leave aside the future sediment terraces. This high erosion rate prevents deposition; most sediments reach the sea.

5.1.2. End of glacials

During approximately the last 10kyr of a glacial period, the rapid warming of temperatures causes the sea level to rise. Upstream rock weathering slowly reduces, and the stream strength loss caused by the increase in sea level results in high fluvial sedimentation.

5.1.3. Interglacials

Due to a more humid climate and milder temperatures, the forest grows, and sediments evolve into soil, protecting the bedrock. Furthermore, dense vegetation coverage was found to reduce the sediment transport distance, effectively increasing sediment deposition [Inb92]; thus, we reduce thermal erosion in our experiments. The primary phenomenon is fluvial erosion, especially downstream sedimentation, favored by vegetation cover, higher precipitation, and low stream strength. These findings from previous geologists are summarized in Table 1.

		Upstream		Downstream	
		Phenomenon	Resulting erosion/deposition	Phenomenon	Resulting erosion/deposition
Glacial	Beginning and maximum	Freeze/Thaw	Thermal phenomena (erosion + rock deposition)	Low sea level Scarce steppe vegetation	Fluvial erosion (deepening of riverbeds)
	Ending	Freeze/Thaw	Reduced thermal phenomena	Increasing sea level	Fluvial erosion + deposition (loss of stream strength)
Interglacial		High sea level	Fluvial erosion (deepening of riverbeds)	High sea level Forested landscape	Deposition of sediments (low stream strength)

Table 1: *The above rules can convert each glacial-interglacial cycle into a specific combination of fluvial and thermal erosion.*

5.2. Simulation Parameter Ranges

In practice, given an input chronology of glacial-interglacial periods, we simulate unerosion back in time by tuning the parameters of our simulation as follows: the thermal erosion coefficient K_{th} is increased in glacial periods from 0.002 to 0.008 to neglect this type of erosion in interglacials. The sedimentation coefficient K_d is tuned in downstream regions to follow sea level (while sea level fluctuates by 150 meters, K_d fluctuates from 0.1 to 3). The precipitation rate p is lowered in glacial periods (from 0.6 to 0.3 m/year), which is set to affect the water flow Q directly.

Tab. 2 shows a summary of all parameters and their range, and Sec. 6.3 shows a case study using these settings.

6. Validation, Control, Results, and Discussion

Our system has been implemented in C++; it uses OpenGL for data visualization, and all simulations run on the CPU. Results were generated on a desktop PC equipped with Intel i9-14900KF Clocked at 3.2GHz, 96GB of DDR5 memory, and an Nvidia GeForce RTX 3080Ti with 12GB of memory. Photorealistic images were rendered in Houdini.

The time complexity of our algorithm is $\mathcal{O}(n \log n)$, with n being

Param.	Definition	Value	Units
h	topography elevation		m
Δt	time step	1000	years
Δx	cell size	[2, 30]	m
p	net precipitation rate	[0, 2]	m/year
U	uplift rate		m/year
m	SPL coefficient	0.4	
n	SPL coefficient	1	
K	erosion coefficient	[0, 1e-2]	$\mathrm{m}^{1-2m}/\mathrm{year}^{1-m}$
Q	water discharge per unit		$\mathrm{m}^2/\mathrm{year}$
K_d	deposition coefficient	[0, 10]	
Q_s	sediment rate		$\mathrm{m}^2/\mathrm{year}$
K_{th}	resistance function	[0, 0.5]	$(1000 \text{ years})^{-1}$

Table 2: *Notations and main parameter values used.*

the grid size because we sort the cells at the beginning of each iteration. The following steps for both fluvial and thermal (un)erosion are $\mathcal{O}(n)$. In practice, one hundred simulation iterations take about 60 seconds for thermal and fluvial unerosion on a 500×500 grid, capturing 2-30m details.

Our formulation for fluvial and thermal erosion with deposition follows a transport equation for which we compute the stability condition (CFL). This condition still holds for unerosion, and deposition does not impact the scheme's stability. For fluvial erosion, a rough estimation of Δt_{max} on the CFL condition ranges 1.42-21.26 kyrs. In real cases, the Δt_{max} should be much higher than our estimation because we consider extreme situations where the drainage area is the whole grid, which is often much bigger than the area in actual cases.

Our algorithm is parameterized by several geological variables that can vary in space and time. The variables include the tectonic uplift U, which is the vertical force responsible for the growth of mountains, the precipitation rate p, fluvial and thermal erosion coefficients K and K_{th}, and deposition rate G. These variables are stored for each time-step t as an additional heightmap layer. Table 2 shows the typical values for these parameters.

We initialize our algorithm with a height $h(t_0)$ and Dirichlet boundary conditions that fix the elevation of the terrain at user-specified locations. In practice, we only require this boundary condition for at least one terrain node. We allow the elevation of this bound to vary over time to mimic the changes in sea level that occur with significant climatic variations, for example, over the glacial cycles of the last million years.
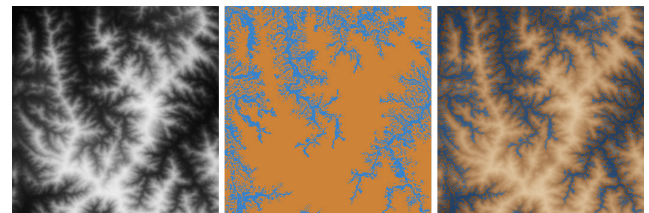

Figure 2: *Fluvial erosion and deposition on an input terrain (left). The intensity of yellow indicates areas where erosion is stronger than deposition, and the blue shows the opposite (middle). Deposition is stronger in valley areas (shown in the overlap on the right).*

6.1. Validation

Our unerosion methods relied on improved fluvial and thermal phenomena since we extended fluvial erosion with sedimentation and modified thermal erosion to make it reversible. An example in Fig. 2 shows fluvial erosion and deposition on an input terrain in varying colors. Deposition is usually stronger in valley areas, as shown in the overlap on the right. The intensity of yellow indicates areas where erosion is stronger than deposition, and the blue part shows the opposite (middle).
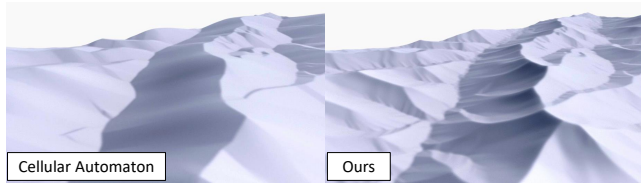
Figure 3: *Comparison of thermal erosion using the cellular automaton method [MKM89] and ours. Our method better preserves geometric features since deposition strictly follows the flow map, which contains the geometric features of the original terrain.*

We also improved thermal erosion (shown in Fig. 3) through a comparison to the classical cellular automaton algorithm [MKM89]. Our method from Sect. 4 better preserves terrain geometric features by following the slope direction, avoiding the smoothing effect of the diffusion-like cellular method.
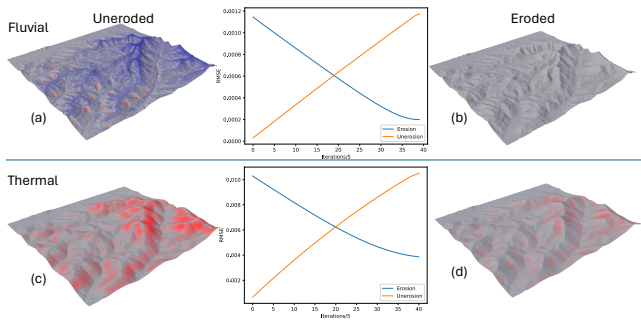

Figure 4: *This numerical validation shows how our unerosion generates valid past states of a terrain. An initial terrain (not displayed) is uneroded by fluvial (a) and thermal unerosion (c). The orange curves in the middle show how the root mean square error (RMSE) between the uneroded terrain and the original one increases. After 200 iterations, the process stops, and the result is displayed (left column). We then apply the corresponding erosion algorithm and, after 200 iterations, converge to a roughly similar terrain to the input (b,d) with decreasing RMSE shown in blue in the middle column. The color coding shows where the error is localized: grey indicates no change, red is higher, and blue is lower.*

Fig. 4 shows how the two unerosion algorithms can generate valid past states. The initial terrain (not displayed) is uneroded by fluvial (a) and thermal erosion (c). The middle column shows the increasing root mean square error (RMSE) compared to the input
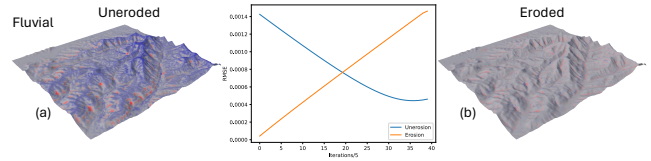

Figure 5: *This experiment shows the lack of accuracy in the classical upwind scheme. An initial terrain (not displayed) is uneroded by fluvial unerosion. After 200 iterations, the process stops, and the result is displayed (left). We then apply the fluvial erosion algorithm for 200 iterations. The final RMSE in this case (blue curve) remains much greater than the results of our method.*

terrain. We then apply the corresponding erosion algorithms back, and the terrains converge to a terrain similar to the input (differences in height shown in blue/red color codes), as indicated by the decreasing RMSE in blue color. As expected, the fluvial erosion (b) has better reversibility (smaller RMSE) than the thermal one (d) as the underlying slope direction does not strongly control it. We also run the same experiment for the fluvial process using the classical upwind scheme. Fig. 5 shows it has lower accuracy than our algorithm.
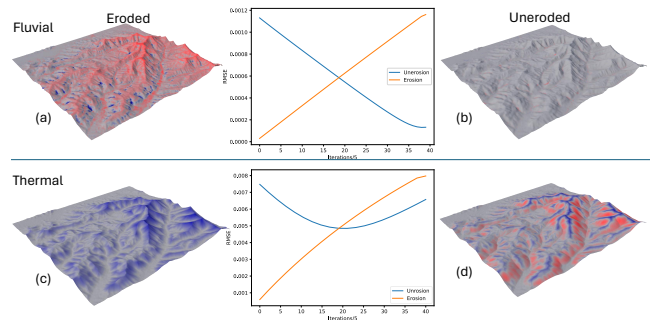

Figure 6: *We also test our algorithm with a reverse experiment of Fig. 4, with the same color coding to localize errors. An initial terrain (not displayed) is eroded by fluvial (a) and thermal erosion (c). The red curves in the middle show how the root mean square error (RMSE) between the uneroded terrain and the original one increases. After 200 iterations, the process stops, and the result is displayed (left). We then apply the corresponding unerosion algorithm for 200 iterations. Although for the fluvial case, it converges to a similar state (b), for the thermal case, it yields a larger RMSE (d), as expected.*

Note that the reverse experiment, consisting of uneroding an eroded terrain, yields a much larger RMSE, as is shown in Fig. 6. This is an expected behavior since erosion has the effect of smoothing out all small geometric features. While unerosion can infer new ones, they cannot exactly match the input, especially for thermal phenomena.

Generating alternative pasts (uneroded terrains) is still valid since they erode to the same present. As presented next, this enables users to tune parameters to explore them.

6.2. User Control

We provide several ways for the user to explore a variety of possible pasts of a terrain. Users can directly tune the unerosion and undeposition rates, expressing a combination of climate, the ground's local nature, and different parameters. Users can utilize a brush tool in the orthographic view of the target terrain. Each parameter can be adjusted on the map by controlling the brush's radius, softness, and depth (refer to the accompanying video). This functionality allows for intuitive control over the location and intensity of the (un)erosion process.

6.2.1. Fluvial unerosion

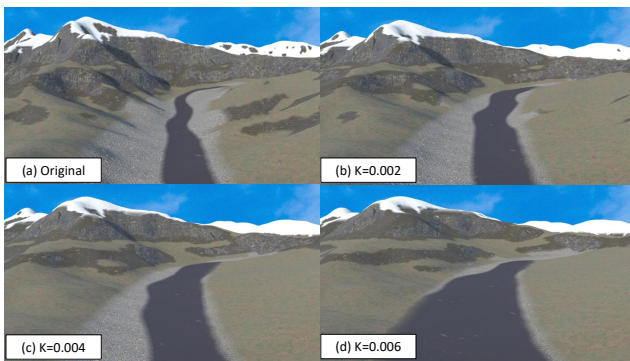First, users can control the net precipitation rate, erosion coefficient, and uplift rate.

Figure 7: *Fluvial un-erosion Tuning the fluvial erosion coefficient K affects the speed of the unerosion process, as shown with 300 iterations (300 kyr) of fluvial unerosion of the input terrain (a). During fluvial unerosion, our algorithm tries to restore the sediments moved away by fluvial erosion. The above figure uses darker areas to represent the restored sediments. As we can see from the figures, with an increasing value of K, more and more sediments would be restored to the river.*

Users can use a brush to edit those values on a map. The first two values determine how fast unerosion goes; the last controls the uplift speed. An example in Fig. 7 shows how erosion coefficient K influences the speed of the unerosion process.

The example in Fig. 8 shows the effect of tuning the parameter deposition coefficient K_d of the fluvial unerosion. The original terrain (top left) is uneroded throughout 300 kyr. The darker areas, which correspond to the river bed, are formed by the deposition of sediments. When we do not consider the un-deposition ($K_d = 0$) during the unerosion process, sediments would not be moved to upstream areas. As a result, they would occupy the whole river. With the increasing value of K_d, the un-deposition process becomes stronger, moving the sediments back to where they originally came from. We also set K_d to extreme values for ablation studies. When $K_d = 32$, the un-deposition is much stronger than unerosion. The sediments are moved away, and the river bed becomes thinner.

6.2.2. Thermal unerosion

An example in Fig. 9 shows how changing the talus angle affects the unerosion algorithm. An initial terrain in (a) is eroded over 100
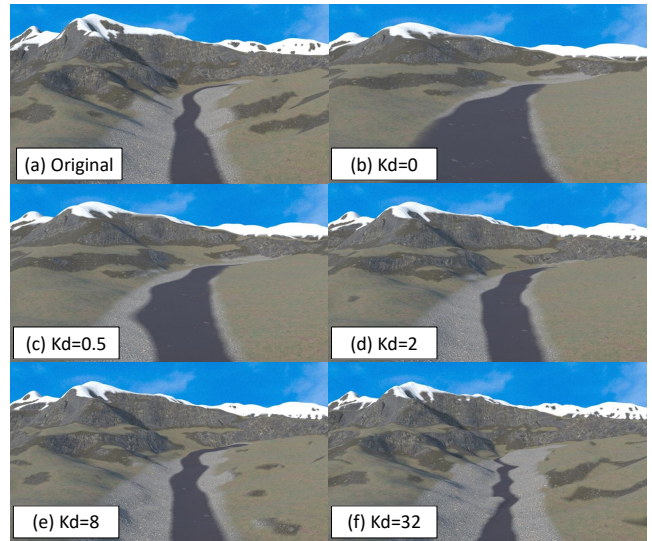

Figure 8: *Fluvial un-erosion Tuning the deposition coefficient K_d affects the un-deposition of sediments (darker color), as shown with 300 iterations (300 kyr) of fluvial unerosion of the input terrain (top left). Darker areas indicate the river bed, which is formed by the deposition of sediments. Note that for $K_d = 8$, the terrain resembles the input one, meaning that erosion and deposition counterbalanced each other. However, the mountain behind still undergoes a great change, showing that erosion was stronger than deposition in the mountains for the last 300,000 years.*

kyr. Low values of the talus angle ($\theta \approx 15^o$) cause the unerosion to create a narrow river. Elevating this parameter will progressively lead to the algorithm's influence becoming more focused on regions with steep slopes.

Fig. 10 shows the effect of the conditions of thermal un-erosion on the un-eroded terrain. The original terrain is uneroded with all constraints (top), without the boundary condition and the max un-deposition. The terrain leads to unnatural shapes if the additional constraints are not used.

6.3. Case Study on Real, Field Data

Case studies with geologists show whether our model can explain field data, giving some evidence about the fluctuation of riverbed heights over the last million years.

6.3.1. Tautavel Plain, 0-814 kyr

We first chose Tautavel Valley in southern France, which is a region of low tectonic activity exempt from any glacial erosion. Its topography is fully explained by combining fluvial and thermal phenomena with a very low uplift (2.5e-5 m/y). The drop in the sea level reached 150 m there during the worst part of some glacials [RBO*06]. Thus, it influenced the deposition/erosion cycles in the valley much more than the uplifting of the Pyrenees mountains. The local climatic fluctuations (Fig. 11) are deduced
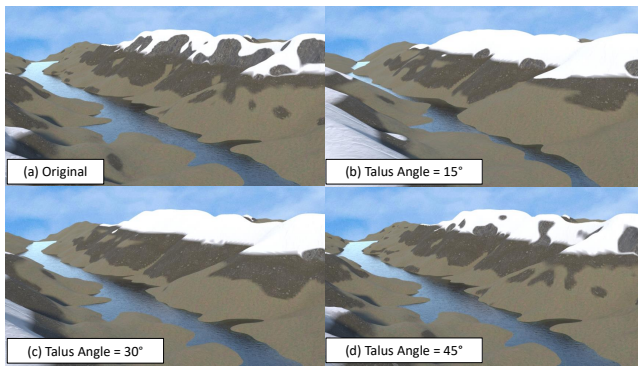
Figure 9: *We run thermal unerosion of the terrain in (a) while changing the talus angle. The effects of thermal unerosion greatly depend on this parameter. For low values (15 degrees), there is still thermal unerosion happening at the brink of the lands. As a result, these places would keep receiving material and narrow the river. For higher values (45 degrees), only the cliff part of the mountain would be affected by erosion. For the rest, they are only affected by un-deposition and did not undergo big changes.*
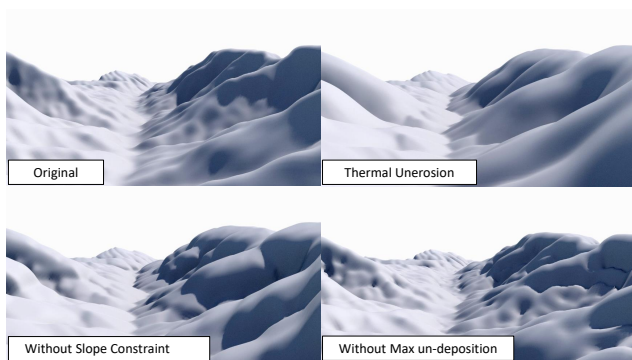

Figure 10: *Effect of constraints on our novel thermal unerosion method. The original terrain (top left) uneroded with all constraints (top right, α set to 1), without slope constraint (bottom left) and without maximal un-deposition rate (bottom right). Without slope constraint, the terrain's slope would constantly become huge and leave some step-like shapes on the terrain; without max un-deposition, there would be many holes on the surface.*

from Arago cave infilling, spanning 600 kyr (90-690 ka). The numerical data was extracted with a kyr time step from the closest continuous marine record off the Balearic Islands (drill ODP 975) while taking into account the sea surface palaeotemperature data reconstructed from the Foraminifers [GMMK13] and adapting it to land temperature from nowadays mean annual difference between both locations.

Lastly, geologic research reported field evidence on the presence of four stepped alluvial terraces showing the height of the riverbed at different time periods, the older one being 30 meters above nowadays river level. They could be dated thanks to either Electron Spin Resonance dating, palaeomagnetic direction, or correlation with the
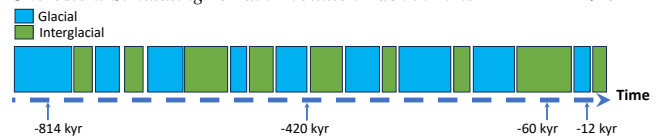

Figure 11: *Chronology of climatic periods in Tautavel Valley.*
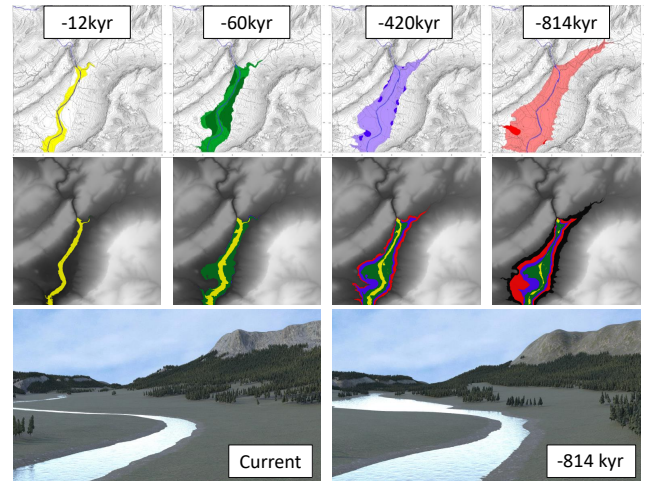

Figure 12: *First row: Data showing sedimental terraces over time (top row), with the field evidence in a darker color and the full terrace guessed by geologists in a lighter color. Second row: Unerosion simulated result at the same points in time (from left to right - 12 kyr, -60 kyr, -420 kyr, -814 kyr). The colors correspond to the levels [m]: yellow 0-4, green: 4-8, blue: 12-20, black: 20 and higher.*

cave or other deposits. Geologists reported an age of around 12 kyr for the first terrace (+ 4m), 60 kyr for the second one (+ 12m), 420 kyr for the third one, and 814 kyr for the fourth terrace (+20 m). See Figure 12, top row.

Starting from the modern topography of the terrain, we used our unerosion model for the corresponding periods of time, using the rules and parameter fluctuation described in Sect. 5. We had to use two maps at two different scales to compute changes in terrain height in the valley at a good resolution while considering the sediments being brought in from upstream or entrained downstream outside the map.

Since there are no pictures of terrains hundreds of thousands of years old, we compare our results with published geological observations (e.g., the local field data) from [LPS14] (maps reproduced at the top of Fig. 12). We find that the past states we predict are valid possible pasts since they can be eroded back to present-day terrain that matches the actual terrain we started with. We observe that the simulated maps fit the field observations very well, particularly regarding the location of the deposits. Altitudes coincide between both sets of maps. Deposits on both sides of the valley correspond to current observations and imply homogeneous uplifting. The difference in the surface of the deposits increases with their age in the simulations. It may result from lacunous field observations, from parameters to adjust in the simulations, or, more probably, from the anthropic impact of cultivation and building through time.
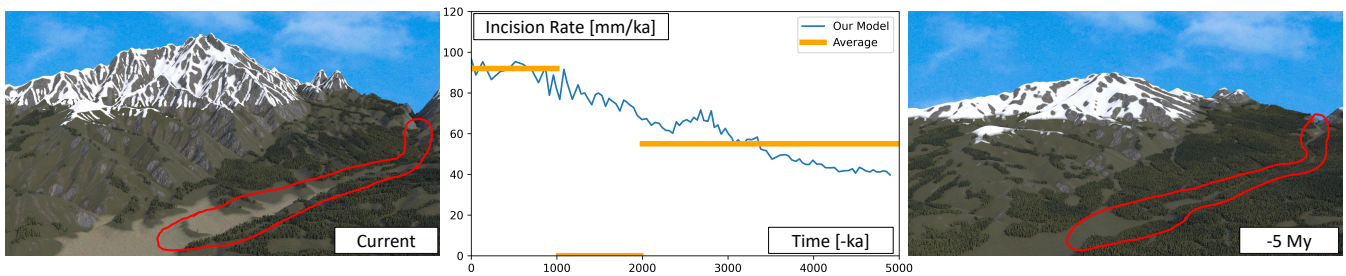
Figure 13: *The central figure is a line graph comparing the predicted incision rates from our model with the incision rates derived from geological observations. The orange line represents the average incision rates over three distinct periods as calculated from the geological data, and the blue curve illustrates the incision rates predicted by our model. Each data point corresponds to the incision rate during a complete glacial and interglacial cycle. The highlighted areas in the figures on the left and right are the specific sections of the Têt River area under our study.*

6.3.2. Conflent Region, 0-5000 kyr

We show that our model can elucidate the evolution of river landscapes in mountainous areas over a span of several million years. We selected the Têt River in the Canigò Massif region, which has experienced significant geological influences, including fluvial and thermal phenomena, alongside notable tectonic uplift (250 mm/ky) over the past 5 million years.

Geological research [CDGL22] has provided estimates of the average incision rates in this river's catchment over the last 5 million years. Incision rate refers to the rate at which a river vertically erodes its bed, thereby deepening its channel through erosional processes. Influential factors on this rate include water flow, sediment load, and regional tectonic activity. The study's methodology for determining incision rates involved dating river-lain deposits in caves that are now above today riverbed.

Utilizing climatic data spanning over one hundred glacial and interglacial cycles from the past 5,000,000 years [LR05], our model predicts the incision rates according to the fluctuations and rules outlined in Sect. 5. This prediction is based on changes in elevation over time, averaged across multiple locations along the river.

Our findings (see Fig. 13) are compared with published geological data [CDGL22]. For the incision rates, geologists have identified three distinct periods of incision between 5 Ma and the present: from 5 to 2 Ma, the average incision rate was 55 mm/ka; from 2 to 1 Ma, the rate was close to zero, as evidenced by overlapping datings of cave levels relative to the current river level; and from 1 Ma to the present, the rate increased to 92 mm/ka. Our model's results align closely with the geological data for the periods from 5 to 2 Ma and from 1 Ma to the present. The incision rate predicted by our model corresponds well with these observed rates, with an acceleration since 1 Ma due to higher climatic overprint.

Discrepancies arise in the period between 2 and 1 Ma. These anomalies in incision rate are potentially attributable to tectonic influences. Between 2 and 1 Ma, the river part may have been temporarily disconnected from the uplifting by activating the faults between the two adjacent mountain areas. As a result, the adjacent mountain areas were uplifting, while the river area was unaffected by incision since it was in subsidence. Another possible reason may

also partly derive from the accuracy of the datings on the sites between 1 and 2 Ma. The fact is that two different cavities, both 110 m above today's river level, gave two different ages for their infilling: 2.23 ± 0.23 Ma and 1.20 ± 0.286 Ma. Geologists deduced relative stability during this period but also pinpointed different phenomenons that may have biased the results (among others, an older infilling introduced secondarily in one of the caves).

6.4. Comparisons

Prior work on fluvial (un)erosion does not consider deposition, corresponding to setting $K_d = 0$ in our model. The main novelty comes from the un-erosion (Fig. 8), where the sediments are carved and sent to their upstream origin. Fig. 5 shows that our scheme improves accuracy compared to previous upwind discretization. Fig. 3 compares with cellular automation-based methods.

6.5. Limitations

Our method has several limitations. First, terrains are made of folded layers of various materials with different erosion behavior. Our results would be much more accurate if our unerosion algorithms were applied to a volumetric earth-crust model, such as the one used in [CCB*18]. In particular, not accounting for various materials prevents us from reversing time for small-scale phenomena such as canyons, fairy chimneys, natural bridges, etc. With our current model, we could easily take advantage of the sediment maps to better constrain unerosion algorithms, enabling only sediments to be brought back up slopes or rivers. Second, our method tends to predict a smoother version among the possible pasts of terrain. Another limitation comes from the problem definition. It is speculative to assume what the past of a terrain would be, and our method makes only an educated guess with the help of the user. However, such a tool can be a valuable addition to the suite of existing terrain modeling algorithms.

7. Conclusions and Future Work

We proposed a novel, efficient solution for simulating the past terrain topography from the input DEM and hypotheses on the main

erosion phenomena it underwent backward in time. Given the number of plausible, possible pasts for the terrain, our solution was augmented with interactive user control, enabling the user to explore several possible pasts by simply changing the combination and parameters of the unerosion algorithms applied backward in time. This opens the way to the use of our method for movies and games, where the characters could travel back in time while staying at the same place, or for scientific documentaries, where dinosaurs or other past species could be featured at a specific location (with corrected past terrain) where their remains were found.

Future work could address the inversion of other erosion algorithms, such as glacial and wind erosion. Glacial erosion has been a significant erosion factor for many regions on Earth over long periods of hundreds of thousands of years, which is not considered in our method. Using machine learning for generating the inversion may be necessary, as it was for solving the equations forward in time [CJP*23]. We also plan to exploit, adapt, and test other forward and backward discretization techniques, such as BFECC. Also, exploring methods that generate smaller-scale geologic features based on statistics would be interesting.

8. Acknowledgments

References

[ABSC14] AMORIM, RONAN, BRAZIL, EMILIO VITAL, SAMAVATI, FARAMARZ, and COSTA SOUSA, MARIO. "3D geological modeling using sketches and annotations from geologic maps". *SketchBased Interfaces and Modeling*. 2014 3.

[ASA07] ANH, NGUYEN HOANG, SOURIN, ALEXEI, and ASWANI, PARIMAL. "Physically based hydraulic erosion simulation on graphics processingunit". *GRAPHITE '07: Proceedings of the 5th international conference on Computer graphics and interactive techniques in Australia and Southeast Asia*. New York, NY, USA: ACM, 2007, 257–264. DOI: http://doi.acm.org/10.1145/1321261.1321308 2.

[BE14] BENN, DOUGLAS I. and EVANS, DAVID J. A. *Glaciers & glaciation*. Routledge, 2014 5.

[Ben07] BENES, BEDRICH. "Real-Time Erosion Using Shallow Water Simulation". *Workshop in Virtual Reality Interactions and Physical Simulation "VRIPHYS" (2007)*. Ed. by DINGLIANA, JOHN and GANOVELLI, FABIO. The Eurographics Association, 2007. ISBN: 978-3-905673-65-4. DOI: 10.2312/PE/vriphys/vriphys07/043-050 2.

[BF01] BENES, BEDRICH and FORSBACH, RAFAEL. "Layered data representation for visual simulation of terrain erosion". *Proceedings Spring Conference on Computer Graphics*. IEEE. 2001, 80–86. DOI: 10.1109/SCCG.2001.945341 2.

[BFH92] BEAUMONT, CHRISTOPHER, FULLSACK, PHILIPPE, and HAMILTON, JULIET. "Erosional control of active compressional orogens". *Thrust tectonics* (1992), 1–18 3.

[BTHB06] BENES, BEDRICH, TĚŠÍNSKÝ, VÁCLAV, HORNYŠ, JAN, and BHATIA, SANJIV K. "Hydraulic erosion". *Computer Animation and Virtual Worlds* 17.2 (2006), 99–108 2.

[BW13] BRAUN, JEAN and WILLETT, SEAN D. "A very efficient O(n), implicit and parallel method to solve the stream power equation governing fluvial incision and landscape evolution". *Geomorphology* 180-181 (2013), 170–179. ISSN: 0169-555X 2, 3.

[CBC*16] CORDONNIER, GUILLAUME, BRAUN, JEAN, CANI, MARIE-PAULE, et al. "Large Scale Terrain Generation from Tectonic Uplift and Fluvial Erosion". *Computer Graphics Forum*. Proc. EUROGRAPHICS 2016 35.2 (May 2016), 165–175. DOI: 10.1111/cgf.12820. URL: https://inria.hal.science/hal-01262376 2, 3.

[CCB*18] CORDONNIER, GUILLAUME, CANI, MARIE-PAULE, BENES, BEDRICH, et al. "Sculpting Mountains: Interactive Terrain Modeling Based on Subsurface Geology". *IEEE Transactions on Visualization and Computer Graphics* 24.5 (May 2018), 1756–1769. DOI: 10.1109/TVCG.2017.2689022. URL: https://hal.science/hal-01517343 10.

[CDGL22] CALVET, MARC, DELMAS, MAGALI, GUNNEL, YANNI, and LAUMONIER, BERNARD. *Geology and Landscapes of the Eastern Pyrenees. A Field Guide with Excursions*. SPRINGER NATURE, SWITZERLAND, 2022, 57-107 and 355–433. DOI: 10.1007/978-3-030-84266-6 10.

[CGG*17] CORDONNIER, GUILLAUME, GALIN, ERIC, GAIN, JAMES, et al. "Authoring Landscapes by Combining Ecosystem and Terrain Erosion Simulation". *ACM Trans. Graph.* 36.4 (July 2017), 134:1–134:12. ISSN: 0730-0301. DOI: 10.1145/3072959.3073667. URL: http://doi.acm.org/10.1145/3072959.3073667 2.

[CJP*23] CORDONNIER, GUILLAUME, JOUVET, GUILLAUME, PEYTAVIE, ADRIEN, et al. "Forming Terrains by Glacial Erosion". *ACM Transactions on Graphics* 42.4 (July 2023), 1–14. DOI: 10.1145/3592422. URL: https://inria.hal.science/hal-04090644 2, 11.

[EHS00] ERICKSON, GREGG, HARDY, STUART, and SUPPE, JOHN. "Sequential restoration and unstraining of structural cross sections: Application to extensional terrains". *AAPG Bulletin* (2000), 234–249 3.

[GCR*18] GARCIA, MAXIME, CANI, MARIE-PAULE, RONFARD, RÉMI, et al. "Automatic Generation of Geological Stories from a Single Sketch". *Expressive '18 - The Joint Symposium on Computational Aesthetics and Sketch Based Interfaces and Modeling and Non-Photorealistic Animation and Rendering*. Victoria, Canada: ACM, Aug. 2018, 17–19. DOI: 10.1145/3229147.3229161. URL: https://inria.hal.science/hal-01817923 3.

[GDG*17] GUÉRIN, ÉRIC, DIGNE, JULIE, GALIN, ÉRIC, et al. "Interactive example-based terrain authoring with conditional generative adversarial networks". *ACM Transactions on Graphics (TOG)* 36.6 (2017), 1–13 2.

[GGG*13] GENEVAUX, JEAN-DAVID, GALIN, ERIC, GUERIN, ERIC, et al. "Terrain Generation Using Procedural Models Based on Hydrology". *ACM TOG (Siggraph 2013)* 33.4 (2013) 2.

[GGP*19] GALIN, ERIC, GUÉRIN, ERIC, PEYTAVIE, ADRIEN, et al. "A Review of Digital Terrain Modeling". *Computer Graphics Forum* 38.2 (2019), 553–577. DOI: 10.1111/cgf.13657. URL: https://hal.science/hal-02097510 2.

[GMMK13] GIRONE, ANGELA, MAIORANO, PATRIZIA, MARINO, MARIA, and KUCERA, MICHAL. "Calcareous plankton response to orbital and millennial-scale climate changes across the Middle Pleistocene in the western Mediterranean". *Palaeogeography, Palaeoclimatology, Palaeoecology* 392 (2013), 105–116. DOI: 10.1016/j.palaeo.2013.09.005 9.

[Gro99] GROSHONG, RICHARD H. "Structural validation, restoration and prediction". *3D Structural Geology: A Practical Guide to Surface and Subsurface Map Interpretation*. Ed. by SPRINGER Berlin, HEIDELBERG. 1999, 305–372 2.

[GRP*21] GRACIANO, ALEJANDRO, RUEDA, ANTONIO J., POSPÍŠIL, ADAM, et al. "QuadStack: An Efficient Representation and Direct Rendering of Layered Datasets". *IEEE Transactions on Visualization and Computer Graphics* 27.9 (2021), 3733–3744. DOI: 10.1109/TVCG.2020.2981565 2.

[Inb92] INBAR, MOSHE. "Rates of fluvial erosion in basins with a Mediterranean type climate". *CATENA* 19.3 (1992). Selected papers of the 2. ICG Symposium on "Mediterranean Erosion", 393–409. ISSN: 0341-8162. DOI: https://doi.org/10.1016/0341-8162(92)90011-Y. URL: https://www.sciencedirect.com/science/article/pii/034181629290011Y 6.

[KBKŠ09] KRIŠTOF, PETER, BENES, BEDRICH, KŘIVÁNEK, JAROSLAV, and ŠŤAVA, ONDŘEJ. "Hydraulic Erosion Using Smoothed Particle Hydrodynamics". *Computer Graphics Forum (Proceedings of Eurographics 2009)* 28.2 (Mar. 2009), 219–228 2.

[KHM*20] KRS, VOJTECH, HÄDRICH, TORSTEN, MICHELS, DOMINIK L, et al. "Wind Erosion: Shape Modifications by Interactive Particle-based Erosion and Deposition." *SCA (Posters)*. 2020, 9–11 2.

[LD03] LAGUE, DIMITRI and DAVY, PHILIPPE. "Constraints on the long-term colluvial erosion law by analyzing slope-area relationships at various tectonic uplift rates in the Siwaliks Hills (Nepal)". *Journal of Geophysical Research: Solid Earth* 108.B2 (2003) 4.

[LNP*12] LIDAL, ENDRE MØLSTER, NATALI, MATTIA, PATEL, DANIEL, et al. "Geological storytelling". *Computers & graphics* 37 (2012), 445–459 3.

[LPS14] LUMLEY, HENRY DE, PERRENOUD, CHRISTIAN, and SAOS, THIBAUD. "Formations quaternaires de la plaine de Tautavel". *Caune de l'Arago. Tautavel-en-Roussillon, Pyrénées-Orientales, France*. Vol. 1. CNRS Éditions, Paris, 2014. Chap. 4, 247–271 9.

[LR05] LISIECKI, LORRAINE E and RAYMO, MAUREEN E. "A Pliocene-Pleistocene stack of 57 globally distributed benthic δ18O records". *Paleoceanography* 20.1 (2005) 10.

[MDH07] MEI, XING, DECAUDIN, PHILIPPE, and HU, BAO-GANG. "Fast Hydraulic Erosion Simulation and Visualization on GPU". *Pacific Graphics*. Vol. 0. Los Alamitos, CA, USA: IEEE Computer Society, 2007, 47–56. DOI: http://doi.ieeecomputersociety.org/10.1109/PG.2007.27 2.

[MKM89] MUSGRAVE, FOREST KENTON, KOLB, CRAIG E., and MACE, ROBERT S. "The synthesis and rendering of eroded fractal terrains". *ACM SIGGRAPH Computer Graphics* 23.3 (1989), 41–50 2, 4, 7.

[NWD05] NEIDHOLD, B., WACKER, M., and DEUSSEN, OLIVER. "Interactive physically based Fluid and Erosion Simulation". *Proceedings of Eurographics Workshop on Natural Phenomena*. Vol. 1. 2005, 25–32 2.

[PPB*23] PERCHE, SIMON, PEYTAVIE, ADRIEN, BENES, BEDRICH, et al. "Authoring Terrains with Spatialised Style". *Computer Graphics Forum*. Vol. 42. 7. Wiley Online Library. 2023, e14936 2.

[RBO*06] RABINEAU, MARINA, BERNÉ, SERGE, OLIVET, JEAN-LOUIS, et al. "Paleo sea levels reconsidered from direct observation of paleoshoreline position during Glacial Maxima (for the last 500,000 yr)". *Earth and Planetary Science Letters* 252.1-2 (2006), 119–137. DOI: 10.1016/j.epsl.2006.09.033 8.

[RKČ*22] RAJASEKARAN, SUREN DEEPAK, KANG, HAO, ČADÍK, MARTIN, et al. "Ptrm: Perceived terrain realism metric". *ACM Transactions on Applied Perceptions (TAP)* 19.2 (2022), 1–22 2.

[ŠBBK08] ŠŤAVA, ONDŘEJ, BENES, BEDRICH, BRISBIN, MATTHEW, and KŘIVÁNEK, JAROSLAV. "Interactive Terrain Modeling Using Hydraulic Erosion". *Proceedings of the 2008 ACM SIGGRAPH/Eurographics Symposium on Computer Animation*. SCA '08. Dublin, Ireland: Eurographics Association, 2008, 201–210. ISBN: 9783905674101. DOI: 10.5555/1632592.1632622 2.

[SBK09] STAVA, ONDREJ, BENES, BEDRICH, and KRIVANEK, JAROSLAV. "Interactive Hydraulic Erosion on the GPU". *ShaderX 7 - Advanced Rendering Techniques*. Ed. by ENGEL, WOLFGANG. Oxford University Press, 2009 2.

[SPF*23] SCHOTT, HUGO, PARIS, AXEL, FOURNIER, LUCIE, et al. "Large-scale terrain authoring through interactive erosion simulation." *ACM Transactions on Graphics* 42 (2023) 2–4.

[VBHS11] VANEK, JURAJ, BENES, BEDRICH, HEROUT, ADAM, and STAVA, ONDREJ. "Large-Scale Physics-Based Terrain Editing Using Adaptive Tiles on the GPU". *IEEE Computer Graphics and Applications* 31.6 (2011), 35–44. DOI: 10.1109/MCG.2011.66 2.

[WCMT07] WOJTAN, CHRISTOPHER, CARLSON, MARK, MUCHA, PETER J., and TURK, GREG. "Animating Corrosion and Erosion". *Proceedings of the Eurographics Workshop on Natural Phenomena, NPH 2007, Prague, Czech Republic, 2007*. Eurographics Association, 2007, 15–22 2.

[Whi04] WHIPPLE, KELIN X. "Bedrock rivers and the geomorphology of active orogens". *Annual Review of Earth and Planetary Sciences* 32.1 (2004), 151–185 3.

[WT99] WHIPPLE, KELIN X. and TUCKER, GREGORY E. "Dynamics of the stream-power river incision model: Implications for height limits of mountain ranges, landscape response timescales, and research needs". *Journal of Geophysical Research: Solid Earth* 104.B8 (1999), 17661–17674 2, 3.

[YBG*19] YUAN, XIAOPING P., BRAUN, JEAN, GUERIT, LAURE, et al. "A New Efficient Method to Solve the Stream Power Law Model Taking Into Account Sediment Deposition". *Journal of Geophysical Research: Earth Surface* 124.6 (2019), 1346–1365 2, 3.

[YM03] YAMADA, YASUHIRO and MCCLAY, KEN. "Application of geometric models to invert listric fault systems in sandbox experiments: hanging wall deformation and section restoration". *Journal of Structural Geology* 25 (2003), 1551–1560 3.

[ZLB*19] ZHAO, YIWEI, LIU, HAN, BOROVIKOV, IGOR, et al. "Multitheme generative adversarial terrain amplification". *ACM Transactions on Graphics (TOG)* 38.6 (2019), 1–14 2.